Dynamics of ferroelectric thin films described by the transverse Ising model

1996 J. Phys.: Condens. Matter 8 3075

(http://iopscience.iop.org/0953-8984/8/17/018)

J. Phys.: Condens. Matter **8** (1996) 3075–3094. Printed in the UK

Dynamics of ferroelectric thin films described by the transverse Ising model

C L Wang†‡ and S R P Smith‡

† Department of Physics, Shandong University, Jinan, 250100, People's Republic of China
‡ Department of Physics, University of Essex, Wivenhoe Park, Colchester CO4 3SQ, UK

Received 15 December 1995

Abstract. The dynamic properties of thin films described by the Ising model in a transverse field (TIM) have been studied under the random-phase approximation. The frequencies of soft modes and surface modes have been obtained. For films with reduced surface interaction (compared to the bulk), the soft mode corresponds to a surface-like mode in the ferroelectric phase but to a bulk-like mode in the paraelectric phase. Conversely, for films with an enhanced surface interaction, the soft mode is a bulk-like mode in the ferroelectric phase and a surface-like mode in the paraelectric phase. The number of surface-like modes in the ferroelectric phase can be greater than one; the number increases as the temperature approaches the Curie temperature, and does not depend on the in-plane wavevector for a given temperature in the ferroelectric phase. However, there is only one surface-like mode in the paraelectric phase, and its character becomes bulk-like at large wavevector. The surface modes can be clearly seen from the frequency dependence of the dynamic susceptibility; the surface mode pole increases in strength with decreasing film thickness. The frequency dependences of optical reflectivity coefficients have also been obtained. The reflection peaks due to the surface modes lie below the bulk reststrahl band in the ferroelectric phase of films with reduced surface ferroelectricity, and also in the paraelectric phase of films with enhanced surface ferroelectricity; otherwise, they lie within the reststrahl band.

1. Introduction

The transverse Ising model (TIM) was originally introduced by de Gennes [1] to describe the bulk phase transition properties of KDP-type ferroelectrics. Since then this model has been extended to study other systems, such as Jahn–Teller [2] and ferromagnetic systems. Surface influences have been investigated by introducing modification of the interaction strength at the surface of a semi-infinite sample [3–6]. In the past few years, the effect of film thickness on the static properties of a TIM film has been investigated, usually by employing a mean-field approximation (MFA) [7–12] or an effective-field theory [13–15]. These investigations have primarily concerned the Curie temperature, polarization, specific heat and susceptibility. This model has also been extended to study the properties of ferroelectric superlattices [16, 17], and the size effect in the quantum paraelectric phase [18]. The bulk susceptibility calculated from the TIM under the MFA can fit the experimental measurements in an excellent manner [19].

Comparatively less work has been done on the dynamic properties of TIM films. Early studies by Blinc and Žekš in their classic book [20] indicated that the bulk (pseudo-) spin wave is the soft mode—its frequency becomes zero at the phase transition temperature. Later the surface influence on the spin-wave spectrum was obtained for a semi-infinite

0953-8984/96/173075+20$19.50

system [3]. A surface mode has been found in systems with either reduced or enhanced surface interaction. In the ferroelectric phase, more than one surface mode has been found, but in the paraelectric phase only one surface mode has been predicted [3]. The latest work is the calculation of the optical reflectivity coefficient of a 10-layer TIM film [21].

The dynamic behaviour of ferroelectric films has also been studied using Landau theory [3] for a semi-infinite system. A surface mode was found only in the ferroelectric phase for a system with reduced surface interaction, and in the paraelectric phase for a system with enhanced surface interaction, a result whose physical basis is clarified by the present paper. Landau theory has also been extended to study the dynamics of a ferroelectric superlattice [22, 23]—a structure that came into reality a few years ago [24]. The calculation shows the existence of interface modes.

Early far-infrared (FIR) measurements [25] on Rochelle salt showed that a thin film has higher transmission than a thick film, and that extra peaks appear in thin films. Recent FIR measurements [26] on $PbTiO_3$ and PZT film have been carried out, but there was no discussion of size or surface effects. Due to potential applications in optic waveguide devices, several kinds of ferroelectric material have been fabricated into very thin films, and their optical properties have been investigated [27, 28]. The optical properties of rf-sputtered lithium niobate thin film on sapphire and SiO_2/Si substrates have been studied using a high-index rutile prism coupler [29]. Both TE and TM modes have been observed in films of thickness 0.6 μm and 0.2 μm. It was reported [30] that a large quadratic electro-optic effect has been observed from high-quality pulsed laser deposition barium titanate film on a MgO substrate. The transmittance of PZT films obtained from rf magnetron sputtering shows interface oscillations caused by the structure of films, and is influenced by their thickness [31].

In this paper we extend our calculations on static properties [11, 12] to study the linear dynamic response of a TIM film. In the next section, the RPA is applied to get the basic expressions. The soft modes and surface modes are obtained and discussed in section 3. In section 4 we present the dispersion relation, in section 5 the dynamic susceptibility and section 6 the optical reflectivity. The last section is a general summary.

2. Formalism

In order to study the linear dynamic properties of the TIM, we apply a small time- and space-dependent external electric field $E_i(t)$, and write the Hamiltonian in the form [20]

$$H = -\sum_i \Omega_i S_i^x - \frac{1}{2}\sum_{i,j} J_{ij} S_i^z S_j^z - 2\mu \sum_i E_i(t) S_i^z \tag{1}$$

where S_i^x and S_i^z are the x- and z-components of a spin-$\frac{1}{2}$ operator. In hydrogen bond ferroelectrics, $S_i^z = +\frac{1}{2}$ and $S_i^z = -\frac{1}{2}$ represent the occupation by a proton of the two equilibrium positions of the hydrogen bond; Ω_i is the transverse field or tunnelling frequency of the proton and S_i^x the corresponding tunnelling operator; J_{ij} is the intersite interaction between sites i and j, equivalent to a dipole–dipole interaction; μ is the effective dipole moment of each site; and $E_i(t)$ is the applied electric field at site i.

The time-dependent expectation values of the spin variables are designated $\langle \boldsymbol{S}_i \rangle_t$; their Heisenberg equations of motion are (in units of $\hbar = 1$):

$$\frac{\mathrm{d}\langle \boldsymbol{S}_i \rangle_t}{\mathrm{d}t} = -\mathrm{i}\langle [\boldsymbol{S}_i, H] \rangle_t . \tag{2}$$

In the RPA [20], the equations of motion (2) take the form

$$\frac{\mathrm{d}\langle \boldsymbol{S}_i\rangle_t}{\mathrm{d}t} = \langle \boldsymbol{S}_i\rangle \times \boldsymbol{H}_i(t). \tag{3}$$

where the time-dependent molecular field $\boldsymbol{H}_i(t)$ is given by

$$\boldsymbol{H}_i(t) = -\frac{\partial\langle H\rangle_t}{\partial\langle \boldsymbol{S}_i\rangle_t}. \tag{4}$$

These equations are equivalent to the classical free precession of the spins $\langle \boldsymbol{S}_i\rangle_t$ around the instantaneous value of the molecular field $\boldsymbol{H}_i(t)$ at a given site.

Since we are interested in the linear response of the spin system to an external field

$$E_i(t) = E_i \mathrm{e}^{\mathrm{i}\omega t} \tag{5}$$

we can replace $\langle \boldsymbol{S}_i\rangle_t$ by a constant part $\langle \boldsymbol{S}_i\rangle$—which is just the MFA expectation value—plus a small time-dependent deviation $\langle \delta\boldsymbol{S}_i\rangle \mathrm{e}^{\mathrm{i}\omega t}$ from the mean-field solution:

$$\langle \boldsymbol{S}_i\rangle_t = \langle \boldsymbol{S}_i\rangle + \langle \delta\boldsymbol{S}_i\rangle \mathrm{e}^{\mathrm{i}\omega t}. \tag{6}$$

Similarly we have

$$\boldsymbol{H}_i(t) = \langle \boldsymbol{H}_i\rangle + \langle \delta\boldsymbol{H}_i\rangle \mathrm{e}^{\mathrm{i}\omega t} \tag{7}$$

where

$$\langle \boldsymbol{H}_i(t)\rangle = \left(\Omega_i, 0, \sum_j J_{ij}\langle S_j^z\rangle_t\right) \tag{8}$$

$$\langle \delta\boldsymbol{H}_i(t)\rangle = \left(0, 0, \sum_j J_{ij}\langle \delta S_j^z\rangle + 2\mu E_i\right). \tag{9}$$

The equations of motion (3) can now be linearized by using (6) and (7) and keeping only terms that are linear in the deviations $\langle \delta\boldsymbol{S}_i\rangle$ and $\langle \delta\boldsymbol{H}_i\rangle$:

$$\mathrm{i}\omega\langle \delta\boldsymbol{S}_i\rangle = \langle \delta\boldsymbol{S}_i\rangle \times \langle \boldsymbol{H}_i\rangle + \langle \boldsymbol{S}_i\rangle \times \langle \delta\boldsymbol{H}_i\rangle. \tag{10}$$

The term $\langle \boldsymbol{S}_i\rangle \times \langle \boldsymbol{H}_i\rangle$ is identically equal to zero as the average value of a spin is oriented along the direction of its molecular field.

As $\langle S_i^y\rangle = 0$ in both the disordered and the ordered phase, the equations of motion for the components of the spin-deviation vector $\langle \delta\boldsymbol{S}_i\rangle$ become

$$\mathrm{i}\omega\langle \delta S_i^x\rangle - \sum_j J_{ij}\langle S_j^z\rangle\langle \delta S_i^y\rangle = 0 \tag{11}$$

$$\sum_j J_{ij}\langle S_j^z\rangle\langle \delta S_i^x\rangle + \mathrm{i}\omega\langle \delta S_i^y\rangle - \Omega_i\langle \delta S_i^z\rangle + \sum_j J_{ij}\langle S_i^x\rangle\langle \delta S_j^z\rangle = -2\mu E_i\langle S_i^x\rangle \tag{12}$$

$$\Omega_i\langle \delta S_i^y\rangle + \mathrm{i}\omega\langle \delta S_i^z\rangle = 0. \tag{13}$$

Eliminating $\langle \delta S_i^x\rangle$ and $\langle \delta S_i^y\rangle$ from (11)–(13) yields

$$[\omega^2 - \Omega_i^2 - \Delta_i^2]\langle \delta S_i^z\rangle + \Omega_i\langle S_i^x\rangle \sum_j J_{ij}\langle \delta S_j^z\rangle = -2\mu E_i\Omega_i\langle S_i^x\rangle \tag{14}$$

where

$$\Delta_i = \sum_j J_{ij}\langle S_j^z\rangle. \tag{15}$$

We now apply these expressions to an N-layer film, in which the lattice sites are assumed to lie on a simple cubic lattice. The interactions are restricted to nearest-neighbour interactions, in which the interaction constant is J except for for interactions between sites

in a surface layer, when the interaction constant is J_s. The corresponding transverse fields are denoted as Ω and Ω_s. We use an in-plane Fourier transform, i.e.

$$\langle \delta \boldsymbol{S}_i \rangle = \sum_{\boldsymbol{Q}} \langle \delta \boldsymbol{S}_n(\boldsymbol{Q}) \rangle \mathrm{e}^{\mathrm{i}\boldsymbol{Q}\cdot\boldsymbol{r}_n} \tag{16}$$

$$E_i = \sum_{\boldsymbol{Q}} E_n(\boldsymbol{Q}) \mathrm{e}^{-\mathrm{i}\boldsymbol{Q}\cdot\boldsymbol{r}_n} \tag{17}$$

where $\boldsymbol{Q} = (Q_x, Q_y)$ is the in-plane wavevector, and $\boldsymbol{r}_n = (x, y)$ denotes the position of the i-site in the layer n; n denotes the layer number along the $\langle 001 \rangle$ direction with $n = 1, \ldots, N$. Then equation (14) can be transformed as follows:

$$\begin{aligned}[\omega^2 - \Omega_s^2 - \Delta_s^2]\langle \delta S_1^z(\boldsymbol{Q}) \rangle + 4J_s\gamma\Omega_s\langle S_1^x \rangle \langle \delta S_1^z(\boldsymbol{Q}) \rangle + J\Omega\langle S_1^x \rangle \langle \delta S_2^z(\boldsymbol{Q}) \rangle \\ = -2\mu E_1(\boldsymbol{Q})\Omega_s\langle S_1^x \rangle \end{aligned} \tag{18}$$

for the surface layer $n = 1$ with a similar equation for $n = N$, and

$$\begin{aligned}[\omega^2 - \Omega^2 - \Delta_n^2]\langle \delta S_n^z(\boldsymbol{Q}) \rangle + 4J\gamma\Omega\langle S_n^x \rangle \langle \delta S_n^z(\boldsymbol{Q}) \rangle + J\Omega\langle S_{n-1}^x(\boldsymbol{Q}) \rangle \langle \delta S_{n-1}^z(\boldsymbol{Q}) \rangle \\ + \Omega J\langle S_{n+1}^x \rangle \langle \delta S_{n+1}^z(\boldsymbol{Q}) \rangle \\ = -2\mu E_n(\boldsymbol{Q})\Omega\langle S_n^x \rangle \end{aligned} \tag{19}$$

for the bulk layers $n = 2, \ldots, N-1$, where

$$\gamma = \frac{1}{2}[\cos(Q_x a) + \cos(Q_y a)]$$

with lattice constant or layer width a, and

$$\Delta_s = 4J_s\langle S_1^z \rangle + J\langle S_2^z \rangle \Delta_n = J(4\langle S_n^z \rangle + \langle S_{n-1}^z \rangle + \langle S_{n+1}^z \rangle).$$

The spin-wave frequencies or eigenfrequencies $\omega(\boldsymbol{Q})$ are obtained by solving (18) and (19) numerically by setting $E_1 = E_n = 0$.

From equations (18) and (19) we can get the relation between the external perturbation $E_n(\boldsymbol{Q})$ and the pseudo-spin system $\delta P_n(\boldsymbol{Q}) = \varepsilon_0 \chi_n E_n(\boldsymbol{Q})$ and hence the dynamic susceptibility χ_n as

$$\chi_n(\omega, \boldsymbol{Q}) = \frac{2\mathcal{N}\mu\langle \delta S_n^z(\boldsymbol{Q}) \rangle}{\varepsilon_0 E_n(\boldsymbol{Q})} \tag{20}$$

where $\mathcal{N}$ is the number of H bonds or effective dipoles per unit volume, μ is the effective dipole moment, and ε_0 is the vacuum permittivity. For convenience of calculation we define a reduced susceptibility for the layer n as

$$\kappa_n = J\frac{\langle \delta S_n^z(\boldsymbol{Q}) \rangle}{2\mu E_n(\boldsymbol{Q})} \tag{21}$$

which is dimensionless and related to the corresponding macroscopic dielectric susceptibility by

$$\chi_n = \frac{4N\mu^2}{J\varepsilon_0}\kappa_n. \tag{22}$$

Thus we can obtain expressions for the reduced susceptibilities directly from (18) and (19):

$$\left[\frac{\Omega_s^2 + \Delta_s^2 - \omega^2}{\Omega_s\langle S_1^x \rangle} - 4J_s\gamma\right]\kappa_1 - J\kappa_2 = 1$$

for the surface layer and

$$-J\kappa_{n-1} + \left[\frac{\Omega^2 + \Delta_n^2 - \omega^2}{\Omega\langle S_n^x \rangle} - 4J\gamma\right]\kappa_n - J\kappa_{n+1} = 1$$

for the bulk layers. The average susceptibilities are defined by

$$\overline{\kappa} = \frac{1}{N}\sum_{n=1}^{N}\kappa_n \qquad \text{or} \qquad \overline{\chi} = \frac{1}{N}\sum_{n=1}^{N}\chi_n. \tag{23}$$

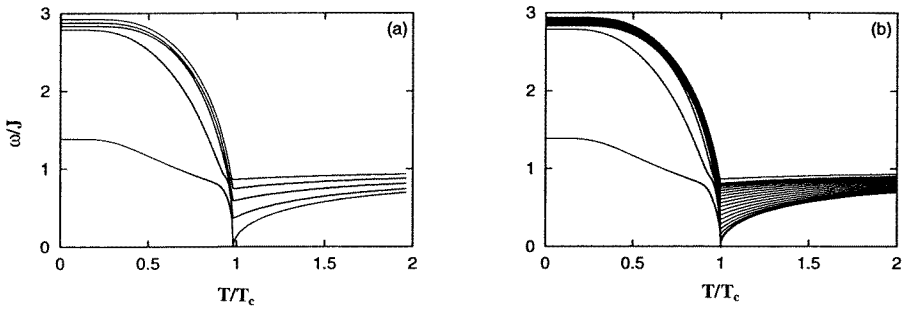

Figure 1. The temperature dependence of the mode frequencies for (a) a 10-layer film and (b) a 40-layer film with reduced surface interaction parameters $J_s/J = 0.5$, $\Omega/J = 1$, $\Omega_s/J = 1$.

As an illustration of the application of the results derived here, we consider the case of optical reflectivity by a thin ferroelectric film. At long wavelength, it is obviously an adequate approximation to represent the properties of the film as those of a medium of thickness $d = Na$ with an average polarization $P = \varepsilon_0\overline{\chi}E$, so that the film behaves as a medium of dielectric constant $\varepsilon = 1 + \overline{\chi}$. The amplitude reflection coefficient for such a film, in vacuum, is [21]

$$R = \frac{(k_0^2 - k^2)\sin(kd)}{(k_0^2 + k^2)\sin(kd) + 2ik_0k\cos(kd)} \tag{24}$$

where k_0 is the vacuum wavevector $2\pi/\lambda$, and k is the wavevector in the film, satisfying the equation $k^2 = \varepsilon\omega^2/c^2$, where c is the velocity of light. The intensity reflection coefficient is $\mathcal{R} = |R|^2$.

3. Soft modes and surface modes

The temperature dependences of the mode frequency and mode configurations are shown in figures 1–6. Three sets of model parameters have been selected to represent typical kinds of film: case (i), a film whose surface ferroelectricity is reduced compared to that of the bulk, i.e. $J_s < 6J/5$ (the factor 6/5 arises because each surface site has only five nearest neighbours, whereas a bulk site has six neighbours); case (ii), a film where the surface interaction is enhanced, $J_s > 6J/5$, in which case there are two phase transitions in thick or infinite systems, one in which the surface layer only becomes polarized, and a second quasi-phase transition in which the polarization spreads to the bulk; and case (iii), a film where the surface interaction is enhanced, but the bulk interaction constant J is insufficient by itself to produce a bulk phase transition ($J < 3\Omega$), so the ferroelectricity in the film is confined to the surface.

Figure 1 shows the temperature dependence of the mode frequencies for a surface-reduced film (i) for 10-layer and 40-layer films. Only the frequencies of the symmetric modes are shown ($N/2$ modes for an N-layer film), because the anti-symmetric modes do not have ferroelectric character. The mode frequencies are normalized by the interaction

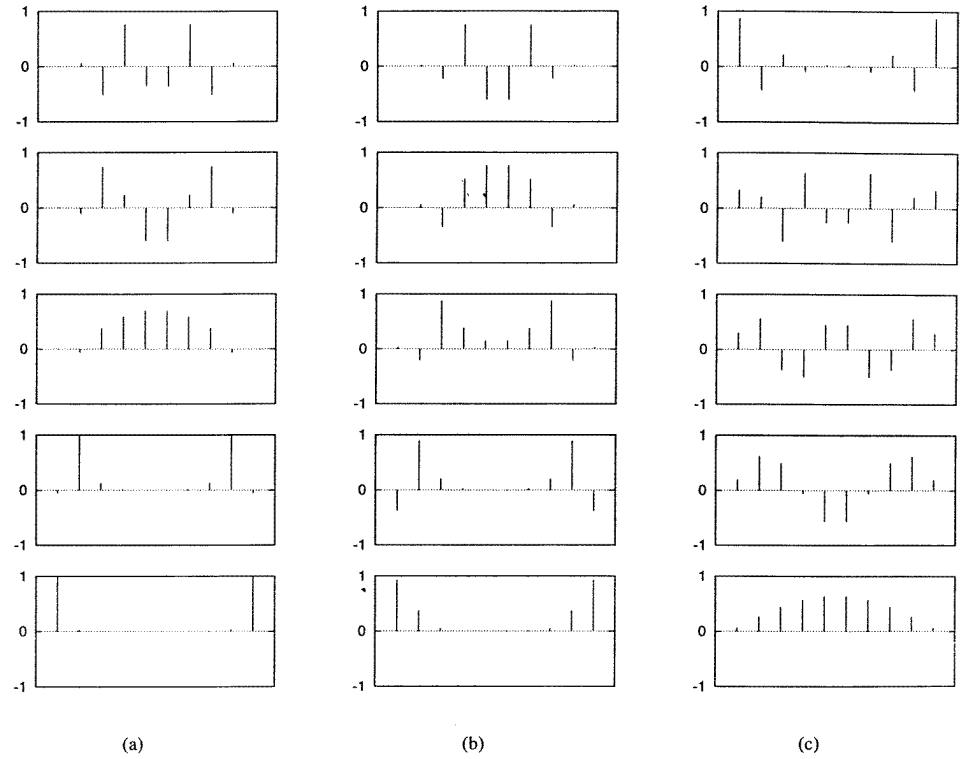

Figure 2. Amplitude profiles of the modes in a 10-layer film shown in figure 1 for (a) a ferroelectric phase, $T/T_{cb} = 0.5$, (b) a ferroelectric phase, $T/T_{cb} = 0.9$ and (c) a paraelectric phase, $T/T_{cb} = 1.5$. The mode frequencies decrease from the top configuration to the bottom.

parameter J, and the temperature scaled by the bulk Curie temperature T_{cb}, defined by the relation

$$\frac{\Omega}{3J} = \tanh\left(\frac{\Omega}{2k_B T_{cb}}\right). \tag{25}$$

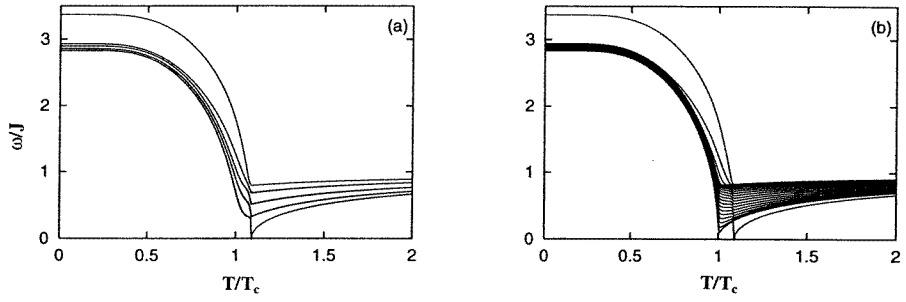

Figure 3. The temperature dependence of the mode frequencies for (a) a 10-layer film and (b) a 40-layer film with enhanced surface interaction parameters $J_s/J = 1.5$, $\Omega/J = 1$, $\Omega_s/J = 1$.

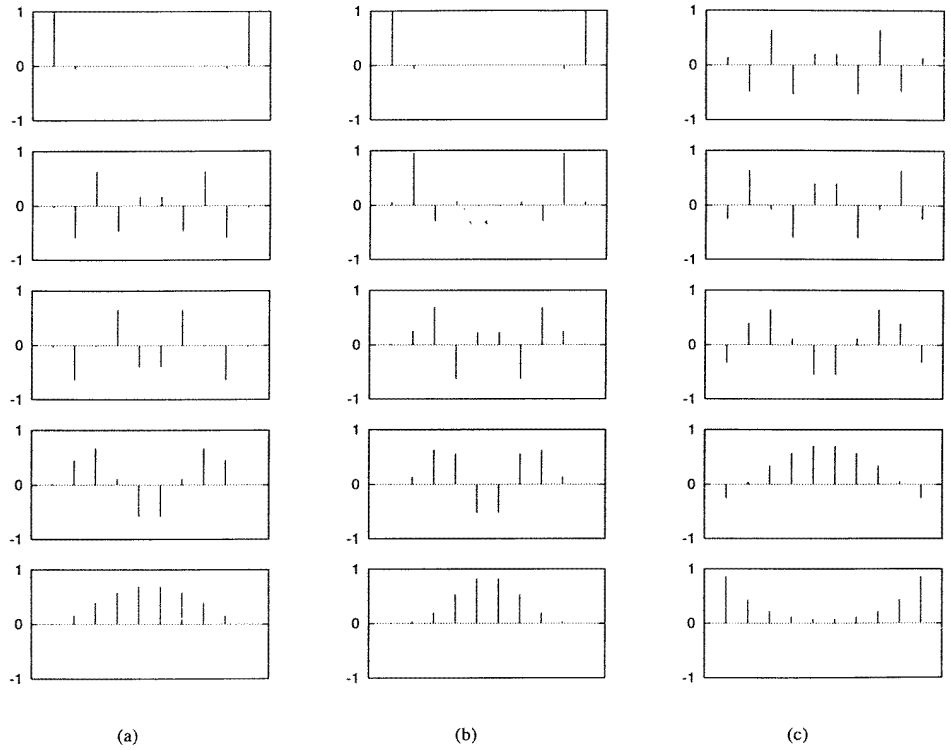

Figure 4. Amplitude profiles of the modes in a 10-layer film shown in figure 3 for (a) a ferroelectric phase, $T/T_{cb} = 0.5$, (b) a ferroelectric phase, $T/T_{cb} = 0.9$ and (c) a paraelectric phase, $T/T_{cb} = 1.5$. The mode frequencies decrease from the top configuration to the bottom.

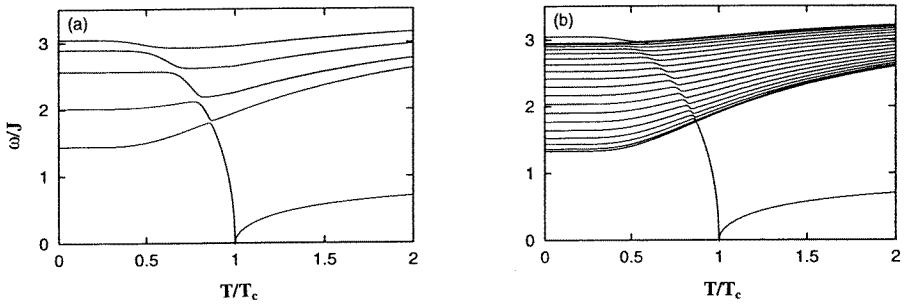

Figure 5. The temperature dependence of the mode frequencies for (a) a 10-layer film and (b) a 40-layer film with enhanced surface interaction with parameters $J_s/J = 1.5$, $\Omega/J = 3.5$, $\Omega_s/J = 1$.

The maximum frequencies at $T \sim 0$ K are $\omega \sim 6J\langle S^z\rangle \sim 3J$, and at high temperature the mode frequencies approach $\omega \sim \Omega$, the transverse field. Figure 2 shows the amplitude profiles of the five even-symmetry modes for the 10-layer film of figure 1 at three temperatures: in the ferroelectric phase at (a) $T/T_{cb} = 0.5$ and (b) $T/T_{cb} = 0.9$, and

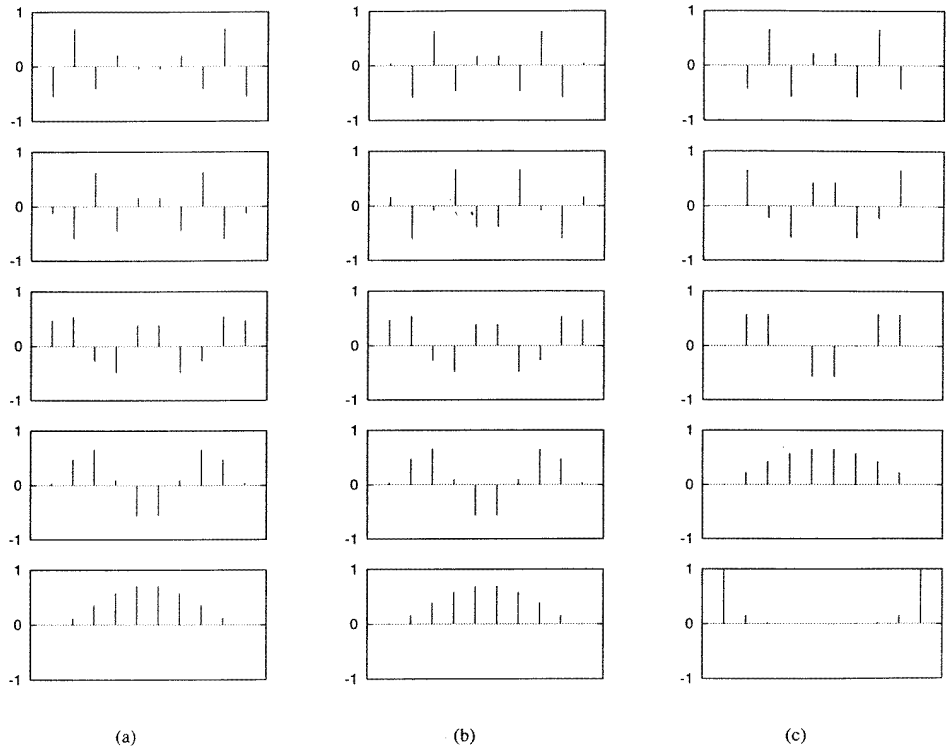

Figure 6. Amplitude profiles of the modes in a 10-layer film shown in figure 5 for (a) a ferroelectric phase, $T/T_c = 0.1$, (b) a ferroelectric phase, $T/T_c = 0.7$ and (c) a paraelectric phase, $T/T_c = 1.5$. The mode frequencies decrease from the top configuration to the bottom.

(c) in the paraelectric phase at $T/T_{cb} = 1.5$. From figure 2(a) it is very easy to see that the two lowest-frequency modes are surface modes, i.e. they have a maximum amplitude at or close to the surface and decay in a quasi-exponential fashion away from the surface. The remaining three modes are confined acoustic-like modes, with wavevectors of approximately k_0, $3k_0$ and $5k_0$, with $k_0 = 2\pi/L$ where L is the layer width. As the temperature approaches $T = 0.9T_{cb}$, the third mode also tends to become surface-like. However, in the paraelectric phase, figure 2(c), the highest-frequency mode is surface-like, and the lowest-frequency mode is a confined mode of wavevector $\sim k_0$. This mode is clearly the soft mode of the system, i.e. it is the mode whose frequency becomes zero at the transition temperature T_{cb}. Immediately below T_{cb} there is a crossover region in which the lowest-frequency mode becomes a surface mode; this crossover can clearly be seen in figure 1. Note that there is little qualitative difference between the 10-layer and 40-layer films, except for the increase in the number of confined modes; in both cases the surface mode has a similar frequency above and below the transition, and the width of the band containing the remaining modes is very similar. In the 40-layer case, the film Curie temperature T_c almost coincides with the bulk Curie temperature T_{cb}. The surface modes can be recognised without much difficulty. There are two surface modes at low temperature, and one more surface mode is split from the bulk region as temperature approaches the Curie temperature. There is only one surface mode in the paraelectric phase in the 40-layer film.

Figure 3 and figure 4 are similar to figures 1 and 2, but for a film with enhanced surface interaction, case (ii). Here, T_c is now above T_{cb}. The surface mode has higher frequency in the ferroelectric phase and lower frequency in the paraelectric phase, and is the soft mode of the phase transition. There is again a crossover region just below T_{cb}, and it is interesting to note in the 40-layer case, figure 3(b), that there is a pseudo-phase transition at T_{cb} when the lowest-frequency confined mode (wavevector $\sim k_0$) nearly reaches zero. As the film thickness increases further, there will in effect be two temperatures at which there are zeros in the frequency spectrum, one corresponding to a bulk mode and the other to a surface mode. This behaviour is different from that of the film with reduced surface interaction (i), in which the Curie temperature T_c shifts up to the bulk Curie temperature as the film thickness increases and the soft mode is always bulk-like.

Figure 5 shows the mode frequencies for case (iii)—enhanced surface interaction, but with the bulk interaction insufficient to cause a phase transition. This differs from case (ii) in that the bulk-like phase transition is absent and so there is only one phase transition, associated with the surface. The temperature data are normalized to T_c for the film. There is only one surface-like mode, which can clearly be distinguished in figures 5(a), 5(b) and 6. Within the ferroelectric phase, this surface mode changes from having the highest frequency at low temperature to having the lowest frequency at high temperature, and the crossover region occupies a range from $T \sim 0.9T_c$ to $T \sim 0.5T_c$.

4. Dispersion relations

The calculations in the last section apply only for the wavevector at $\boldsymbol{Q} = 0$. For a finite in-plane wavevector, the dispersion relations for mode frequency versus wavevector are shown in figures 7 to 9, in which the wavevector is along the [100] direction, or $|\boldsymbol{Q}| = Q_x$. The wavevector is shown in units of $1/\pi a$, where a is the lattice constant. Calculations with general wavevector $\boldsymbol{Q} = (Q_x, Q_y)$ have also been performed, and the general behaviour is not changed very much: the frequency is highest at the boundary of the Brillouin zone along the [110] direction, due to our assumption that the structure is square within the xy-plane. In the following the results and discussions apply to the wavevector along the [100] direction, but the discussion can be applied to other directions with only slight modification.

Figure 7 is for films with reduced surface interaction (case (i)): figures 7(a)–7(c) are for the 10-layer films and figure 7(d)–7(f) are for the 40-layer films. The dashed lines are the corresponding bulk curves: the lower curve is for $Q_z = 0$ and the upper dashed curve is for $Q_z = \pi/a$. In figure 7(a) the temperature is set at $T/T_{cb} = 0.5$, and the two low-lying surface modes are very easy to recognise. When the film thickness increases to 40 layers, as shown in figure 7(d), there are still two surface modes, and their positions are almost unshifted. The increase of film thickness only adds more bulk modes. As the temperature nears the Curie temperature (see figure 7(b) and figure 7(e) for $T/T_{cb} = 0.9$) there are four surface modes, two more than that at $T/T_{cb} = 0.5$, leaving only one bulk mode in the 10-layer film (figure 7(b)). The number of surface modes does not depend on the film thickness, but obviously the number of remaining bulk mode does. Figures 7(c) and 7(f) are presented for the paraelectric phase, with temperature $T/T_{cb} = 1.5$. There is an optic-like surface mode near the Brillouin zone centre at small wavevector which joins the bulk mode band at large wavevector, with the result that there is no distinguishable surface mode near the Brillouin zone boundary in the paraelectric phase. This is still true and more obvious when the film thickness is 40 layers, as shown in figure 7(f).

Figure 8 is for films with strong surface interaction (case (ii)): figures 8(a)–8(c) are for 10-layer films, and figures 8(d)–8(f) for 40-layer films. Figures 8(a) and 8(b) are for

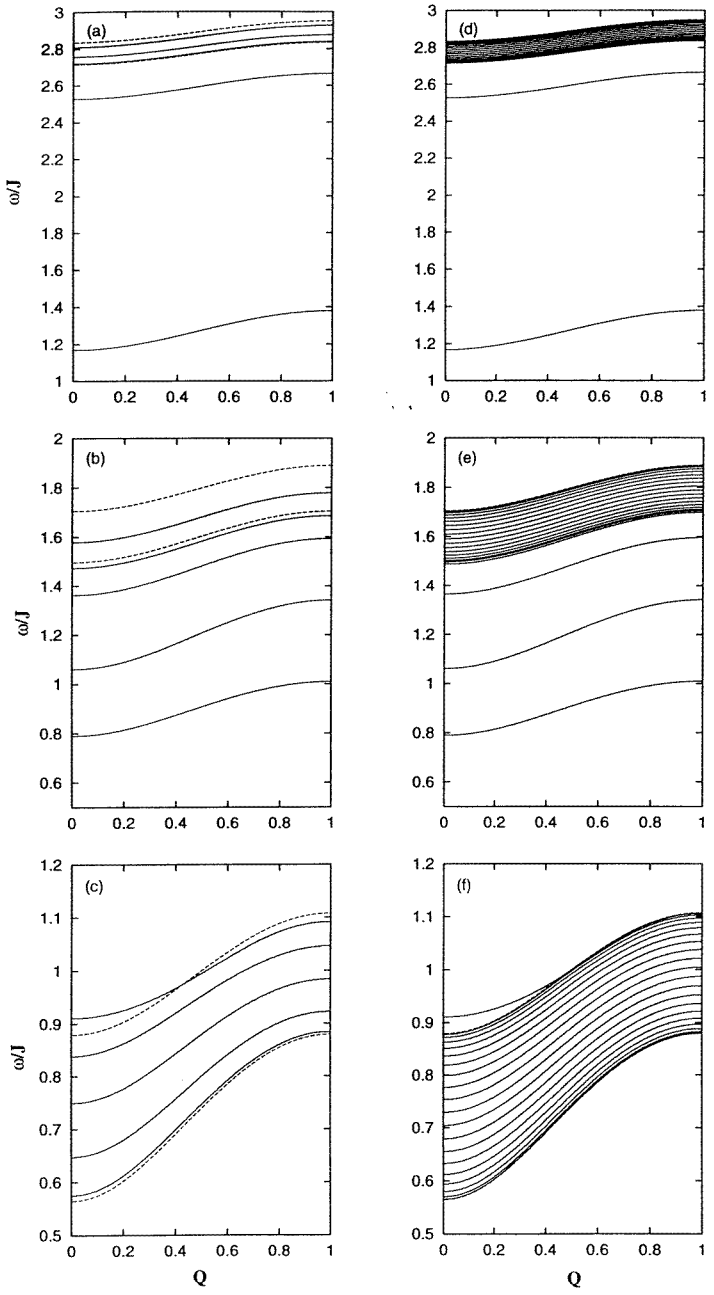

Figure 7. Dispersion diagrams for a film with reduced surface interaction with parameters the same as for figure 1. (a) 10-layer film at $T/T_{cb} = 0.5$, (b) 10-layer film at $T/T_{cb} = 0.9$, (c) 10-layer film at $T/T_{cb} = 1.5$, (d) 40-layer film at $T/T_{cb} = 0.5$, (e) 40-layer film at $T/T_{cb} = 0.9$, (f) 40-layer film at $T/T_{cb} = 1.5$. The dashed lines are the corresponding bulk curves.

the ferroelectric phase, at $T/T_c = 0.5$ and $T/T_c = 0.9$ respectively. There is one surface mode at $T/T_c = 0.5$ for the 10-layer film, and still only one for the 40-layer film at the

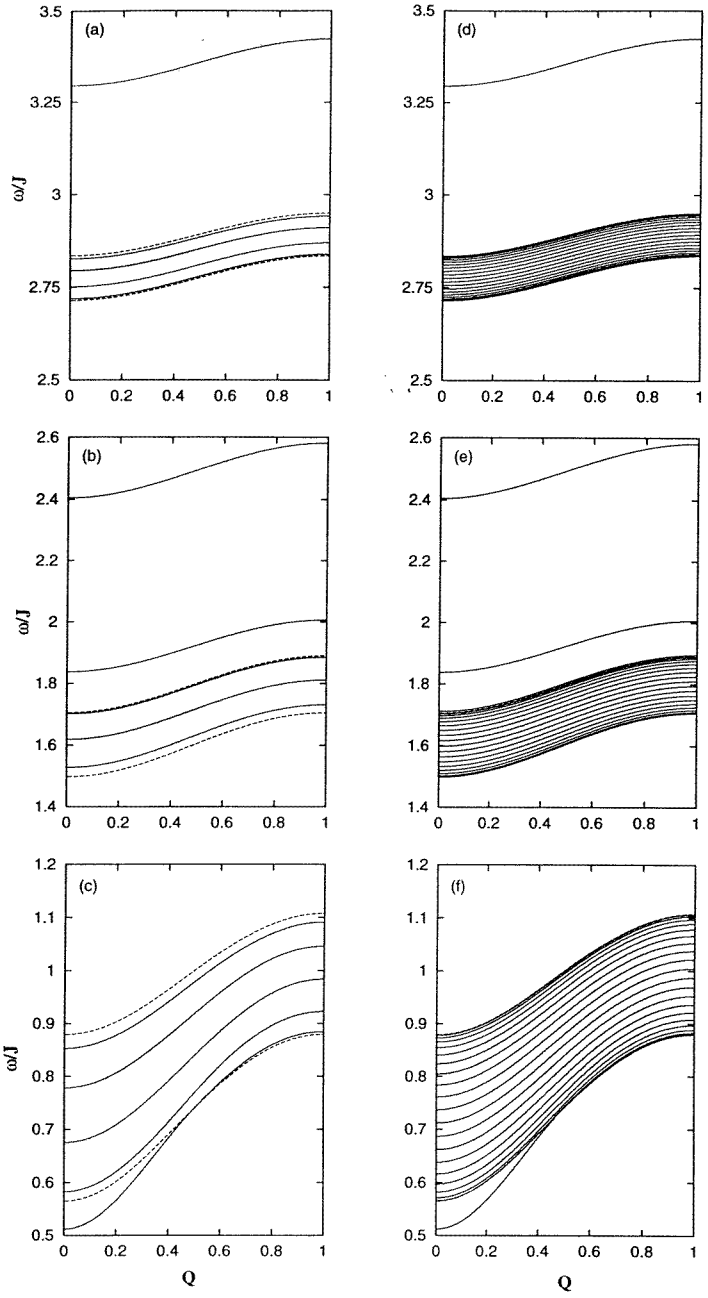

Figure 8. Dispersion diagrams for a film with enhanced surface interaction with parameters the same as for figure 3. (a) 10-layer film at $T/T_{cb} = 0.5$, (b) 10-layer film at $T/T_{cb} = 0.9$, (c) 10-layer film at $T/T_{cb} = 1.5$, (d) 40-layer film at $T/T_{cb} = 0.5$, (e) 40-layer film at $T/T_{cb} = 0.9$, (f) 40-layer film at $T/T_{cb} = 1.5$.

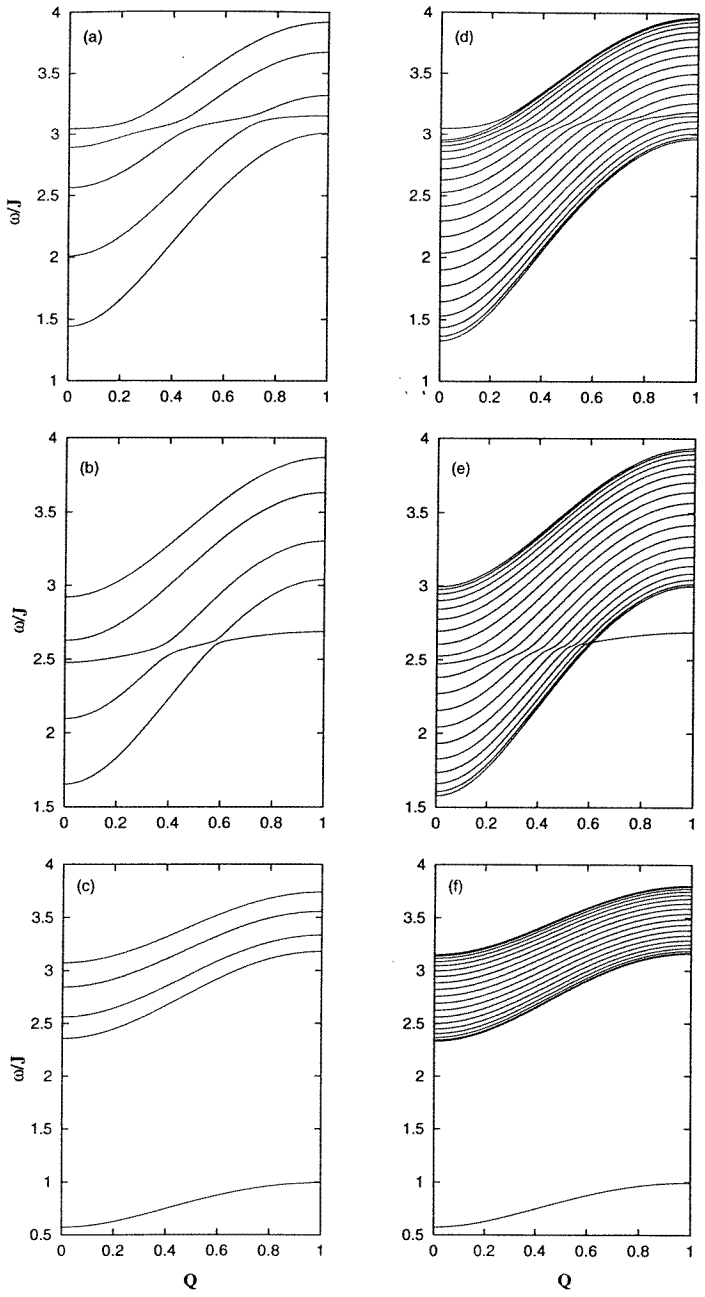

Figure 9. Dispersion diagrams for a film with enhanced surface interaction with parameters the same as for figure 5. (a) 10-layer film at $T/T_c = 0.1$, (b) 10-layer film at $T/T_c = 0.7$, (c) 10-layer film at $T/T_c = 1.5$, (d) 40-layer film at $T/T_c = 0.1$, (e) 40-layer film at $T/T_c = 0.7$, (f) 40-layer film at $T/T_c = 1.5$.

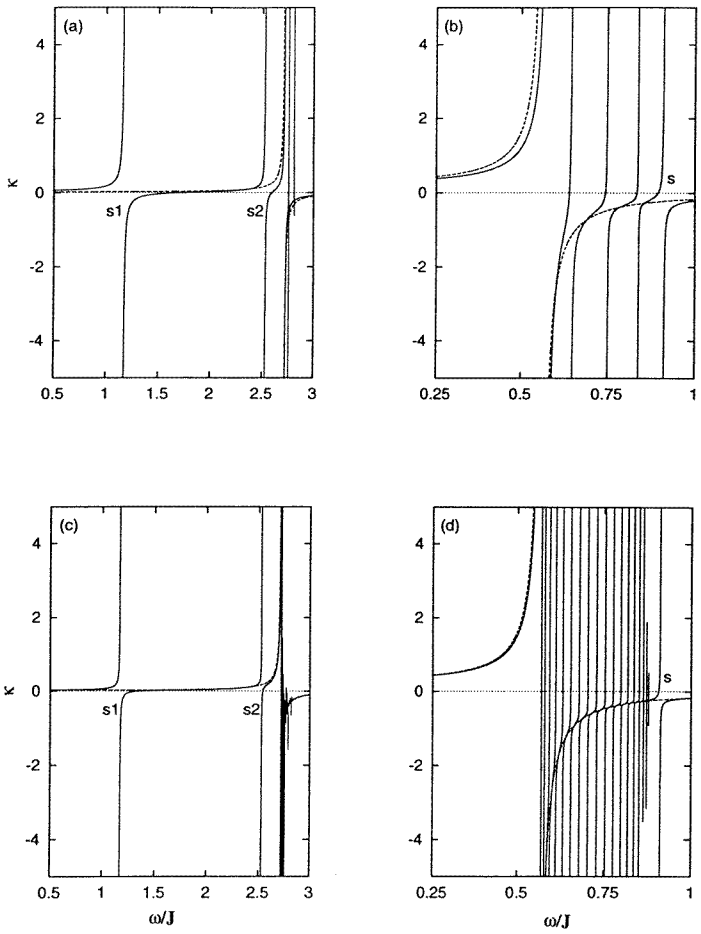

Figure 10. Dynamic susceptibility for a film with reduced surface interaction with parameters the same as for figure 1. (a) 10-layer film at $T/T_{cb} = 0.5$, (b) 10-layer film at $T/T_{cb} = 1.5$, (c) 40-layer film at $T/T_{cb} = 0.5$, (d) 40-layer film at $T/T_{cb} = 1.5$.

same temperature (compare figures 8(a) and 8(d)). One more surface mode appears when the temperature increases to $T/T_c = 0.9$ for the 10-layer film, but two more surface modes appear for the 40-layer film, one very close to the upper bulk mode. In the paraelectric phase, shown in figures 8(c) and 8(f) for $T/T_c = 1.5$, only one surface mode can be found in the small-wavevector region, and this joins the bulk modes at large wavevector, analogously to figures 7(c) and 7(f) but on the lower-frequency side.

Figure 9 is for a film with enhanced surface interaction, corresponding to case (iii) of the last section. Figures 9(a) and 9(d) are for $T/T_c = 0.1$, well below the transition temperature, where there is a single high-frequency surface mode, distinguishable only at small wavevector, which is more obvious in figure 9(d) for the thicker film. In figures 9(b) and 9(e), where the temperature $T/T_c = 0.7$ is still in the ferroelectric phase, the behaviour is quite different from that in figures 9(a) and 9(d). First the surface mode does not exist around small wavevector, but can be picked out near the Brillouin boundary, being

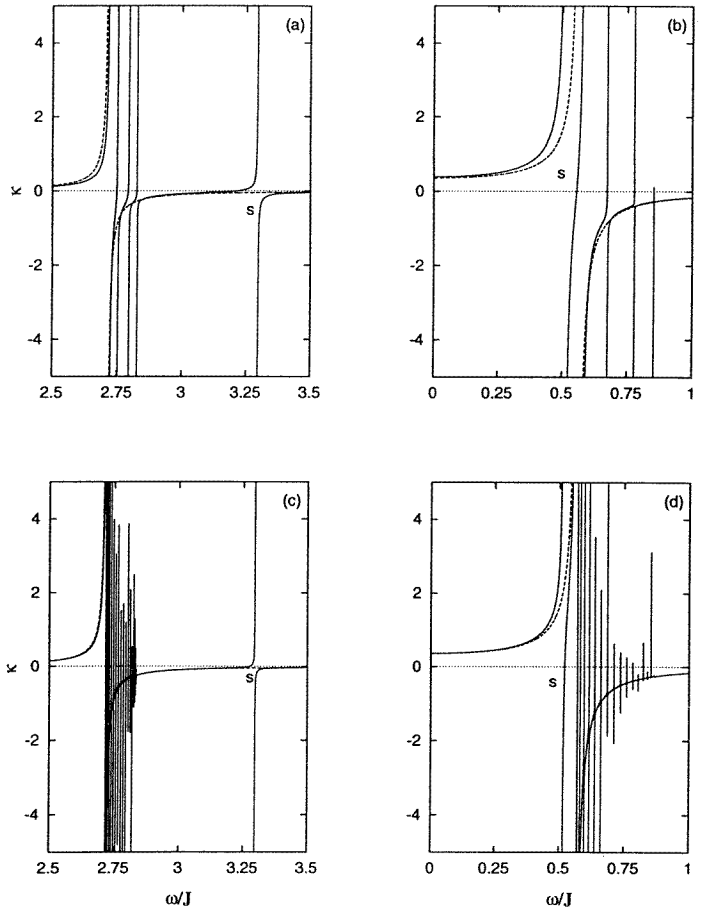

Figure 11. Dynamic susceptibility for a film with enhanced surface interaction with parameters the same as for figure 3. (a) 10-layer film at $T/T_{cb} = 0.5$, (b) 10-layer film at $T/T_{cb} = 1.5$, (c) 40-layer film at $T/T_{cb} = 0.5$, (d) 40-layer film at $T/T_{cb} = 1.5$.

split from the bulk modes beyond a certain wavevector. The second difference is that the surface mode is the lowest-frequency mode, not the highest as in figures 9(a) and 9(d). In the paraelectric phase, figures 9(c) and 9(f) for $T/T_c = 1.5$, the surface mode is quite obvious and very isolated from the bulk modes at low frequency. The frequency of the surface mode is not appreciably affected by the film thickness at any temperature in this case.

5. Dynamic susceptibility

Figures 10–12 show the frequency dependence of the reduced dynamic susceptibility $\kappa(\omega)$ at $\boldsymbol{Q} = 0$ for different film thicknesses and different temperatures. The dashed lines in the figures show the corresponding bulk susceptibility.

Figure 10 shows the susceptibility for films with reduced surface interaction (case (i)). Figures 10(a) and 10(b) are for 10-layer films, and figures 10(c) and 10(d) are for 40-layer

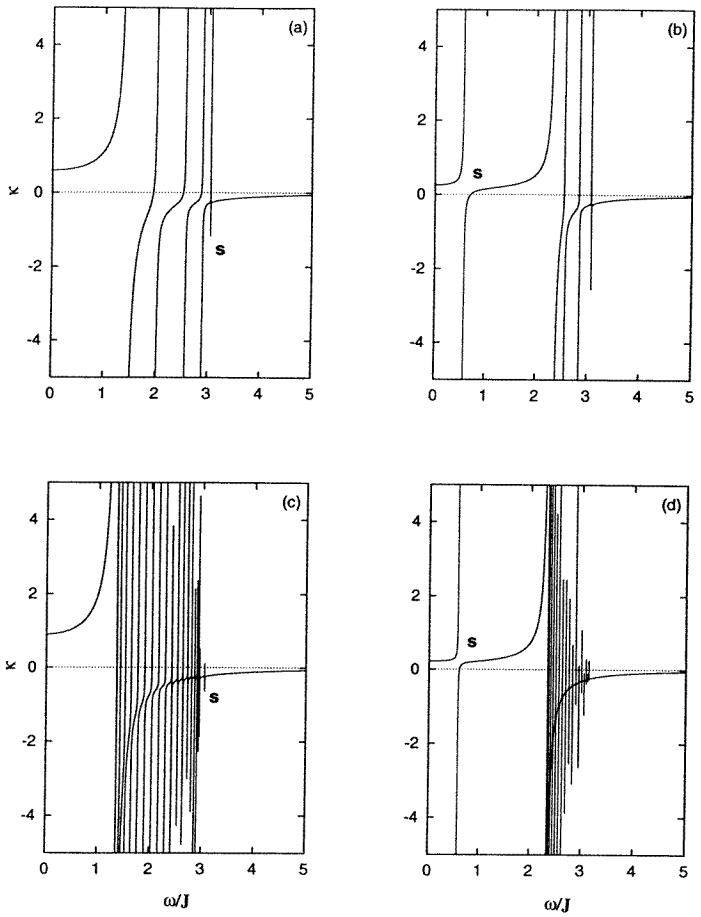

Figure 12. Dynamic susceptibility for a film with enhanced surface interaction with parameters the same as for figure 5. (a) 10-layer film at $T/T_c = 0.1$, (b) 10-layer film at $T/T_c = 1.5$, (c) 40-layer film at $T/T_c = 0.1$, (d) 40-layer film at $T/T_c = 1.5$.

films, and show only the symmetric mode responses. Figure 10(a) is for the ferroelectric phase at $T/T_{cb} = 0.5$; the two surface modes, marked as s1 and s2, lie far below the bulk modes and can be easily recognised. The thinner (10-layer) film has stronger poles than the thicker (40-layer) film. Figure 10(b) is for the paraelectric phase at temperature $T/T_{cb} = 1.5$. The single surface mode, marked s, is now the highest in frequency. The surface modes are more easily recognised in the 40-layer film (figures 10(c) and 10(d)). The increase of film thickness adds more bulk modes, and consequently weakens the strength of the individual poles.

Figure 11 shows diagrams of dynamic susceptibility similar to those of figure 10, but for films with enhanced surface interaction (case (ii)). Only one surface mode appears on the lower-frequency side in the paraelectric phase at $T/T_{cb} = 1.5$; the bulk mode responses merge nearly indistinguishably in the thicker film. Figure 12 shows similar diagrams for case (iii). The strength of the pole corresponding to the surface mode is rather weaker in figure 12(a) than in figure 11(c) in the ferroelectric phase, but is very obvious in the

paraelectric phase. Its frequency is well below that of the bulk modes, and its response does not change appreciably with film thickness.

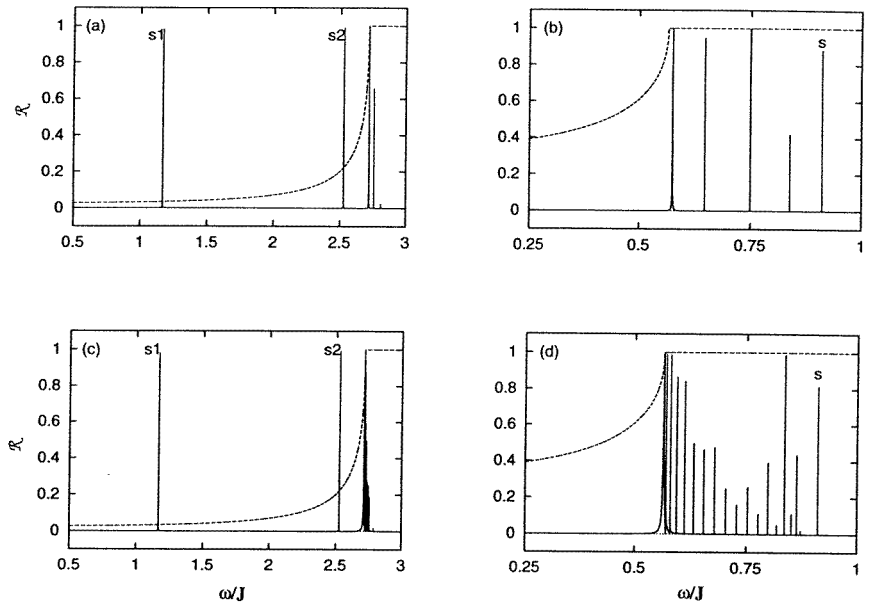

Figure 13. The optical reflectivity coefficient for a film with reduced surface interaction with parameters the same as for figure 1. (a) 10-layer film at $T/T_{cb} = 0.5$, (b) 10-layer film at $T/T_{cb} = 1.5$, (c) 40-layer film at $T/T_{cb} = 0.5$, (d) 40-layer film at $T/T_{cb} = 1.5$.

6. Optical reflectivity

Following the calculation of the dynamic susceptibility in the last section, we extend the calculation to obtain the optical (i.e. far-infrared) reflection coefficients. The results are presented in figures 13 to 15. A general feature is that this spectrum consists of a series of relatively narrow peaks, separated from each other by rather large spectral intervals with no appreciable reflection. It is worth noting that when the film thickness d is very small and the frequency is not close to a pole in the susceptibility, we can get the reflectivity coefficient from equation (24) in a very simple form:

$$\mathcal{R} = \frac{1}{4}\left(\frac{\omega^2}{c^2}\right)(1-\varepsilon)^2 d^2$$

where c is the velocity of light. As d is very small, this will result in very weak reflectivity if the frequency is not near a mode frequency.

The reflection coefficient of film with reduced surface ferroelectricity (case (i)) is shown in figure 13. Figure 13(a) is for a 10-layer film in the ferroelectric phase at temperature $T/T_{cb} = 0.5$. There are two very obvious surface modes which are marked as s1 and s2. The dashed line is the corresponding reflectivity for the bulk material. The remaining three reflection peaks correspond to bulk modes, and all lie in the reststrahl band of the bulk material. This can be seen more easily from figure 13(c), which shows the reflection coefficient of a 40-layer film at the same temperature, in which the two peaks from the

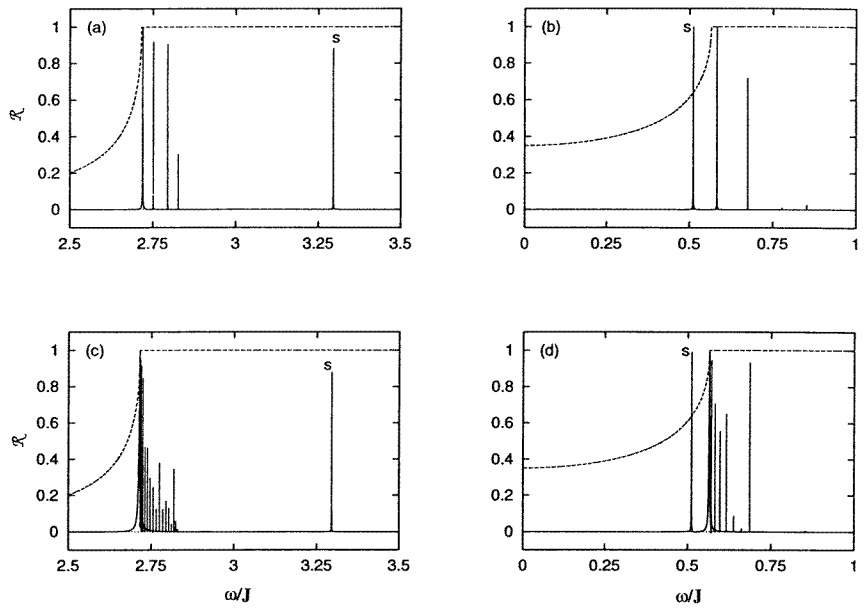

Figure 14. The optical reflectivity coefficient for a film with enhanced surface interaction with parameters the same as for figure 3. (a) 10-layer film at $T/T_{cb} = 0.5$, (b) 10-layer film at $T/T_{cb} = 1.5$, (c) 40-layer film at $T/T_{cb} = 0.5$, (d) 40-layer film at $T/T_{cb} = 1.5$.

surface modes scarcely change their position and strength but more reflection peaks from the bulk mode appear. Figure 13(b) is the reflection coefficient of a 10-layer film in the paraelectric phase with $T/T_{cb} = 1.5$. The reflection peak from the surface mode is not as obvious as that in the ferroelectric phase. All of the reflection peaks lie within the reststrahl band of the bulk reflectivity. As the film thickness increases, more bulk modes appear and the lowest bulk mode shifts to lower frequency. Changing the film thickness does not obviously change the position and strength of the reflection peaks due to the surface mode.

The reflection coefficient of a film with enhanced surface ferroelectricity (case (ii)) is shown in figure 14. The reflection coefficient in the ferroelectric phase at $T/T_{cb} = 0.5$ is shown in figure 14(a). The reflection peak from the surface mode is isolated on the high-frequency side, and is marked by s; the other four modes are very close and at lower frequency. When the film thickness increases, as shown in figure 14(c) for a 40-layer film at the same temperature, the surface mode is still apparent, but more bulk modes appear around the reststrahl edge. In the paraelectric phase, the surface mode appears as the lowest-frequency mode. Again, an increase of film thickness increases the number of bulk modes and shifts the lowest bulk mode much nearer to the mode frequency of the bulk material.

Figure 15 shows the anomalous case (iii) discussed in section 3. Here the temperature scale is the film Curie temperature as there is no corresponding bulk transition. In the ferroelectric phase, we would expect from the discussion in the last two sections that the surface mode is the highest in frequency. However, in both figure 15(a) and figure 15(c), it is very difficult to distinguish the surface mode, and there is almost no difference when the film thickness increases from 10 to 40 layers. However, in the paraelectric phase, the reflection from the surface mode is quite obvious as it is split from the bulk mode and far below the other bulk modes, and the film thickness has no influence on the surface mode

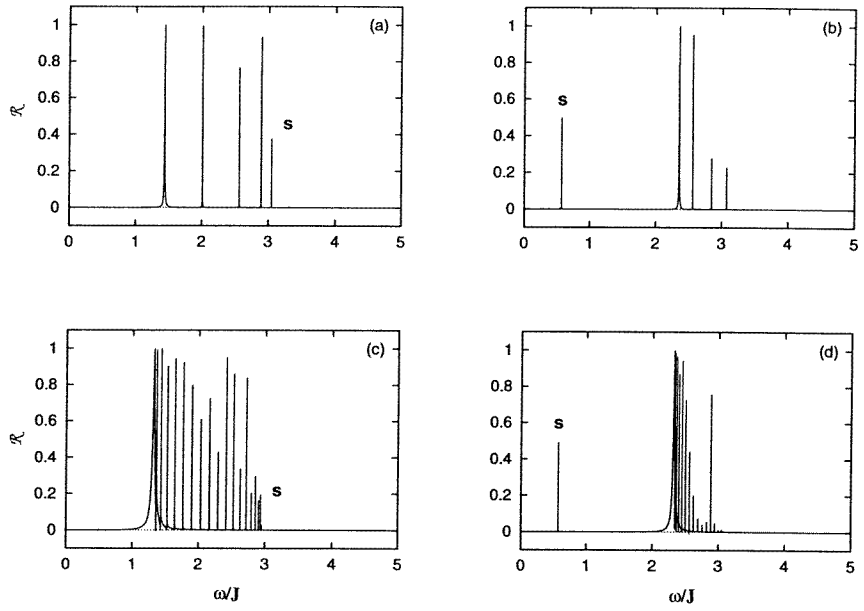

Figure 15. The optical reflectivity coefficient for a film with enhanced surface interaction with parameters the same as for figure 5. (a) 10-layer film at $T/T_c = 0.1$, (b) 10-layer film at $T/T_c = 1.5$, (c) 40-layer film at $T/T_c = 0.1$, (e) 40-layer film at $T/T_c = 1.5$.

as also happens in case (i) and case (ii).

7. Discussion and conclusion

Early investigations on the semi-infinite TIM system also found one surface mode in the paraelectric phase, which joins the bulk mode at large wavevector [3]. This is in agreement with our calculation shown in figures 7(f) and 8(f). It was also found that in the ferroelectric phase, the frequency of the surface mode is above that of the bulk modes if the surface interaction is enhanced, and below that of the bulk modes otherwise. All of these findings show no conflict with our calculation of dispersion relation curves.

However, it seems that there are differences from the results obtained from Landau theory [3] for the semi-infinite system. Here, it was shown that the surface mode for a system with reduced surface polarization can only exist in the ferroelectric phase, or around the Curie temperature and in the paraelectric phase for a system with enhanced surface polarization. The absence of surface modes, which are predicted by our TIM model, is the result of the assumption that Landau theory is valid only around the Brillouin zone centre. In other words, Landau theory is concerned only with the lowest-frequency quasi-acoustic modes, and so if we compare only the acoustic-like modes in our calculation with the Landau theory calculations there is no disagreement.

As a summary, the soft mode still exists in the film geometry. For a film with reduced surface interaction, the soft mode is a surface mode in the ordered phase and becomes a bulk mode in the paraelectric phase. For a film with enhanced surface interaction, the soft mode is a bulk mode at low temperature, but changes into a surface mode at around the Curie temperature and at higher temperature. For a thick film, there may appear two points

at which the mode frequency softens, one at the bulk Curie temperature and another at the surface transition temperature, as happens in the semi-infinite system. The number of surface modes may be more than one in the ferroelectric phase, and more surface modes appear as the temperature approaches the Curie temperature. In the ferroelectric phase, these modes are acoustic-like (i.e. at lower frequency) for films with reduced surface interaction, and optic-like (i.e. at higher frequency) for films with enhanced surface interaction. In the paraelectric phase, only one surface mode exists. It is acoustic-like for films with reduced surface interaction; otherwise it is an optic-like mode. As the in-plane wavevector increases, all mode frequencies increase. The number of surface modes in the ferroelectric phase does not change with wavevector, but does change in the paraelectric phase. The surface mode disappears at large wavevector, so there is no surface mode near the Brillouin boundary in the paraelectric phase. The results for dynamic susceptibility and optical reflection coefficients show that the film thickness has almost no obvious influence on the position and strength of the surface modes. The surface mode is easier to observe in the ferroelectric phase in a film with reduced ferroelectric interaction, and in the paraelectric phase for a film with enhanced surface interaction.

In our analysis, we have ignored the effects of damping. Damping can be introduced phenomenologically into equation (3) in a way analogous to that used in magnetic resonance [20]. This considerably increases the complexity of the calculations, particularly in the ferroelectric phase (in [20], such calculations were performed for the bulk paraelectric phase only), and we have here therefore concentrated on the undamped modes and responses. The principal effects of damping will be to increase the linewidths of the excitations, thus reducing the amplitudes of the reflectivity peaks whilst keeping the integrated response relatively unchanged.

References

[1] de Gennes P G 1963 *Solid State Commun.* **1** 132
[2] Sandercock J R, Palmer S B, Elliott R J, Hayes W, Smith S R P and Young A P 1972 *J. Phys. C: Solid State Phys.* **5** 3126
[3] Cottam M G, Tilley D R and Žekš B 1984 *J. Phys. C: Solid State Phys.* **17** 1793
[4] Cottam M G and Tilley D R 1989 *Introduction to Surface and Superlattice Excitations* (Cambridge: Cambridge University Press)
[5] Sarmento E F, Tamura I, de Oliveira L E M and Kaneyoshi T 1984 *J. Phys. C: Solid State Phys.* **17** 3195
[6] Tamura I, Sarmento E F and Kaneyoshi T 1984 *J. Phys. C: Solid State Phys.* **17** 3207
[7] Aguilera-Granja F and Moran-Lopez L 1990 *Solid State Commun.* **74** 155–8
[8] Wang C L, Zhong W L and Zhang P L 1992 *J. Phys.: Condens. Matter* **3** 4743
[9] Sy H K 1993 *J. Phys.: Condens. Matter* **5** 1213
[10] Wang C L, Zhang P L, Wang Y G, Qu B D and Zhong W L 1994 *Ferroelectrics* **152** 213
[11] Wang C L, Smith S R P and Tilley D R 1994 *J. Phys.: Condens. Matter* **6** 9633
[12] Wang C L, Smith S R P and Tilley D R 1995 *J. Magn. Magn. Mater.* **140–144** 1729
[13] Sarmento E F and Tucker J W 1993 *J. Magn. Magn. Mater.* **118** 133–41
[14] Wang X Z, Jian X Y and Wang J J 1992 *J. Phys.: Condens. Matter* **4** 3651
[15] Wang X Z and Zhao Y 1993 *Physica* A **193** 133
[16] Qu B D, Zhong W L and Zhang P L 1994 *Phys. Lett.* **189A** 419
[17] Qu B D, Zhong W L and Zhang P L 1995 *Japan. J. Appl. Phys.* **34** 4114
[18] Song T K, Kim J and Kwun S I 1995 *Solid State Commun.* **72** 143
[19] Hemberger J, Lunkenheimer P, Viana R, Bohmer R and Loidl A 1995 *Phys. Rev.* B **52** 13159
[20] Blinc R and Žekš B 1974 *Soft Modes in Ferroelectrics and Antiferroelectrics* (Amsterdam: North-Holland)
[21] Smith S R P, Tilley D R and Wang C L 1995 *Integrated Ferroelectr.* **9** 49
[22] Schwenk D, Fishman F and Schwabl F 1990 *Ferroelectrics* **104** 349
[23] Schwenk D, Fishman F and Schwabl F 1990 *J. Phys.: Condens. Matter* **2** 5409
[24] Tsurumi T, Suzuki T, Yamane M and Daimon M 1994 *Japan. J. Appl. Phys.* **33** 5192

[25] Gerbaux X, Hadni A and Kitade A 1989 *Phys. Status Solidi* a **115** 587
[26] Fedorov I, Petzelt J, Železný V, Komandin G A, Volkov A A, Brooks K, Huang Y and Setter N 1995 *J. Phys.: Condens. Matter* **7** 4313
[27] Kamalasanan M N, Chandra S, Joshi P C and Mansingh A 1991 *Appl. Phys. Lett.* **59** 3547
[28] Wood V E, Busch J R, Ramamurthi S D and Swart S L 1991 *J. Appl. Phys.* **71** 4557
[29] Huang C H J and Rabson T A 1991 *Proc. 3rd Int. Symp. on Integrated Ferroelectrics (Colorado Springs, CO, 1991)* p 278
[30] Kim D H and Kwok H S 1995 *Appl. Phys. Lett.* **67** 1803
[31] Chang D A, Lin P and Tseng T Y 1995 *Japan. J. Appl. Phys.* **34** 4854